Seung Yoon Lee, Dongseop Lee, Yueping Zhang, Wonbin Hong, and Nima Ghalichechian

History and Latest Progress in Antenna Packaging Technology

Part 2: Emerging materials and solutions.

xxxxx

In Part 2 of this review article, we discuss antenna-on-chip (AoC) solutions for highly integrated millimeter-wave (mm-wave) devices in wireless communications. We also analyze multiple solutions to address the low antenna efficiency of Si substrates, one of the key limitations of AoCs. This is followed by entirely new antenna-in-package (AiP) configurations using glass core substrates for fifth generation (5G) or beyond 5G communications and the unique antenna-on-display (AoD) concept for mobile devices. Finally, we conclude with emerging materials and packaging techniques for future mm-wave applications. In Part 1 of this review article, we discussed multilayer organic and inorganic materials for antenna packaging and its applications. We also introduced AiP-based phased-array systems integrated with radio frequency (RF) transceiver dies.

Digital Object Identifier 10.1109/MAP.2025.3570830

INTRODUCTION

To enable millimeter-wave (mm-wave) wireless systems, antenna-in-package (AiP) and antenna-on-chip (AoC) technologies have emerged as a key evolution, allowing the integration of antennas with radio-frequency (RF) and digital circuitry in a compact form factor [1], [2], [3], [4], [5]. The AiP solutions for mm-wave communications were discussed in detail in part 1 of this review article [1]. Recently, AoC solutions have gained popularity in Si technologies, such as CMOS or Si-germanium bipolar CMOS (SiGe BiCMOS), by integrating antennas with front-end circuitry on the same die, as illustrated in Figure 1(a). AoC eliminates the need for lossy flip-chip interconnects and wire bonds. Common AoC designs include dipole [6], [7], monopole [8], [9], inverted-F [10], Yagi–Uda [11], slot [12], [13], [14], [15], and patch antennas [16], [17]. Dipole and Yagi–Uda antennas are preferred for their differential characteristics, enabling direct connection to RF front-end differential circuits

without lossy baluns [18]. Semiconductor technologies such as CMOS [12], [19], SiGe BiCMOS [6], [11], SiC [20], [21], and III-V compounds like GaAs [22] and InP [23], [24] can be accessed through collaborations with foundry companies. In-house microfabrication can also be employed for the implementation of AoCs.

In addition, antenna packaging that uses a glass-core interposer is becoming attractive in the design and utilization of mm-wave 5G and terahertz (THz) 6G modules due to its ability to form fine pitch lines and spaces close to Si with low cost, as illustrated in Figure 1(c) and (d). Figure 1(c) shows an AiP using glass as the dielectric, while Figure 1(d) illustrates a 2.5D AiP structure with interposers. The 2.5D architecture uses glass or Si interposers to enhance lateral interconnect density, overcoming the limitations of 2D packaging. Glass-core substrate technology offers a coefficient of thermal expansion (CTE) closely matched to the Si die, along with excellent electrical resistivity, low dielectric loss, and high thermal stability [25], [26]. Meanwhile, as mobile displays increase and human body parts affect the performance of antennas, placing antenna arrays in mobile phone bezels has become challenging. As future 5G smartphones that demand more antenna modules, AiP or AoC solutions may face spatial limitations. Alternatively, embedding optically invisible antennas into a display has become a valid option, referred to as *antenna on display* (*AoD*) [Figure 1(e)] [27], [28]. The advantage of AoD is that display-integrated antennas experience less electromagnetic attenuation because they are less affected by the metal frames and chassis of mobile devices.

Advances in antenna systems, including organic and inorganic AiP, Si-based phased arrays, AoC, and AoD, are closely linked to progress in heterogeneous and monolithic packaging technology. A good understanding of next-generation packaging methods is necessary, including novel materials, 2.5D packaging, fan-out wafer-level packaging (FOWLP) [Figure 1(b)], interposers, and through-Si vias (TSVs) for the future integration of antennas.

Part 2 of this two-part article is organized as follows. The "Silicon-Based Antennas" section discusses the virtue of Si, AoC architectures, and methods for improving AoC efficiency. The "Glass-Based Antenna Solutions" section explores glass-core AiP and the AoD concept. The "Future Research Thrusts" section addresses future research directions, including FOWLP-based AiP, chiplet integration, interposers, and new materials. The "Mm-Wave 5G and Beyond: Key Takeaways" section provides a summary of the key points from parts 1 and 2, and the "Conclusions" section concludes the article.

Si-BASED ANTENNAS

Si is abundant, making up 27.7% of Earth's crust. Si can be easily purified to have extremely low impurity concentrations ($<10^{10}$ impurities/cm^3). It can be doped with both n- and p-type impurities, offering a high dynamic range (less than 10^{14}–10^{21} cm^{-3}). Additionally, Si can be easily grown or deposited in three material forms: crystalline, polycrystalline, and amorphous, each with various applications [29]. These advantages have made Si widely used in semiconductor integrated circuit (IC) chips.

ON-CHIP ANTENNAS

AoCs extend Si substrates into the antenna region, providing advantages over other material-based approaches [18]. AoC eliminates the need for heterogeneous integration, allowing antenna arrays to integrate monolithically with RFICs without high-loss flip-chip interconnects or wire bonds in the mm-wave band. AoCs provide superior fabrication precision, enabling more accurate prediction of antenna characteristics in the mm-wave band using commercial CMOS, SiGe BiCMOS, and III-V semiconductor processes, or microfabrication techniques. Implementing the AoC simplifies the impedance matching problem because the IC components, including a low-noise amplifier and a power amplifier, don't necessarily need to be matched to 50 Ω. Instead, the antenna and circuit can be co-designed to conjugate match each other, avoiding the need for a complex matching network. Finally, AoCs can potentially be integrated with advanced materials that are not traditionally used in antenna structures but can provide multifunctionality. Examples include electrical [30], [31], [32], [33] and mechanical [34], [35] phase-change materials (PCMs), which are discussed in the "Future Research Thrusts" section.

Studies have been conducted to improve the gain and efficiency of AoCs due to Si's lossy characteristics and high permittivity. One approach involves creating an air cavity in Si through postprocessing. Lee et al. [13] achieved a high-efficiency 1 × 8 array using a deep reactive ion-etching process on a 60-GHz coplanar folded slot antenna array, as shown in Figure 2(a). The single-element efficiency was 93%, with the array showing 67% total efficiency and an 11.3-dBi gain. The technique of forming an air cavity at the bottom has been applied in various antenna topologies, including patch [16], [36], dipole [6], and Yagi [11] antennas, to achieve high efficiency by leveraging air

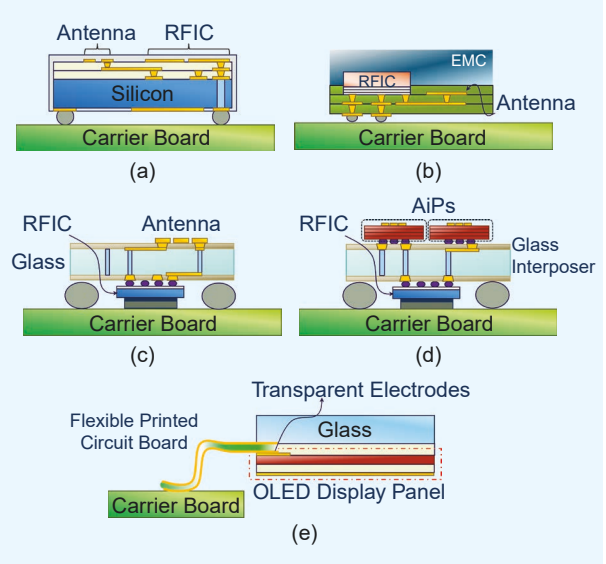

FIGURE 1. Stack-up of a novel antenna packaging architecture. (a) AoC stack-up. (b) Fan-out wafer-level packaging AiP. (c) Glass-core AiP. (d) 2.5D AiP with glass interposer. (e) Stack-up of AoD technology. RFIC: RF integrated circuit; EMC: epoxy mold compound.

as a dielectric. Reducing the cavity footprint or filling it with other dielectrics [16] is also of interest, as the air cavity compromises mechanical robustness. Additionally, studies have used superstrates [37], [38] or dielectric resonator antennas (DRAs) [19], [21], [39], [40] to enhance radiation efficiency. Li et al. [37] introduced a patch-array structure that achieved a high measured efficiency of 83% at 60 GHz by incorporating a fused silica superstrate through a microelectromechanical systems SU-8 suspension [Figure 2(b)]. Zihir et al. [38] implemented phased arrays on an Si substrate packaged with a quartz superstrate, achieving radiation efficiencies of 50% at 60 GHz. However, superstrates or DRA technologies require additional heterogeneous integration in monolithically integrated phased-array systems.

As illustrated in Figure 2(c), researchers have introduced metasurfaces, specifically, on-chip electromagnetic bandgaps [14] and high impedance surfaces [41], which have demonstrated a realized gain of –0.6 and –2.5 dBi, respectively. However, unlike replacing Si with air cavity or DRA techniques, the integration of metasurfaces into AoC is generally challenging to achieve efficiencies higher than 50% due to the inherent high permittivity and loss of doped Si. In recent years, research on AoCs in the THz band has increased, indicating continuous fabrication improvements and potentially promising applications in THz bands [42], [43], [44]. The use of bumping technology in fabricating AoCs is novel, which can be viewed as an important paradigm shift from planar to nonplanar AoC fabrication. More importantly, the microbump structure creates new operating mechanisms and retains the advantages of planar antennas for integrability, manufacturability, and cost, thereby making them particularly suitable for THz AoC solutions. For example, Deng et al. [43] developed a 300-GHz high-efficiency AoC using microbumps [Figure 2(d)]. Radiation efficiency, peak realized gain, and impedance bandwidth were improved dramatically from 15.9% to 41.1%, 1.91 to 8.67 dBi, and 15.6 to 39.6 GHz, respectively.

With the rapid growth of high data rate applications, there has been a paradigm shift for the integration of antennas with RFICs using CMOS, SiGe BiCMOS, and compound semiconductor technologies. Given the limited transmit power, high propagation losses, and the need for high data rate in the mm-wave band, highly efficient phased arrays are critical. AoC solutions integrate antennas on the same die as other circuits using semiconductor technology, while AiP solutions implement

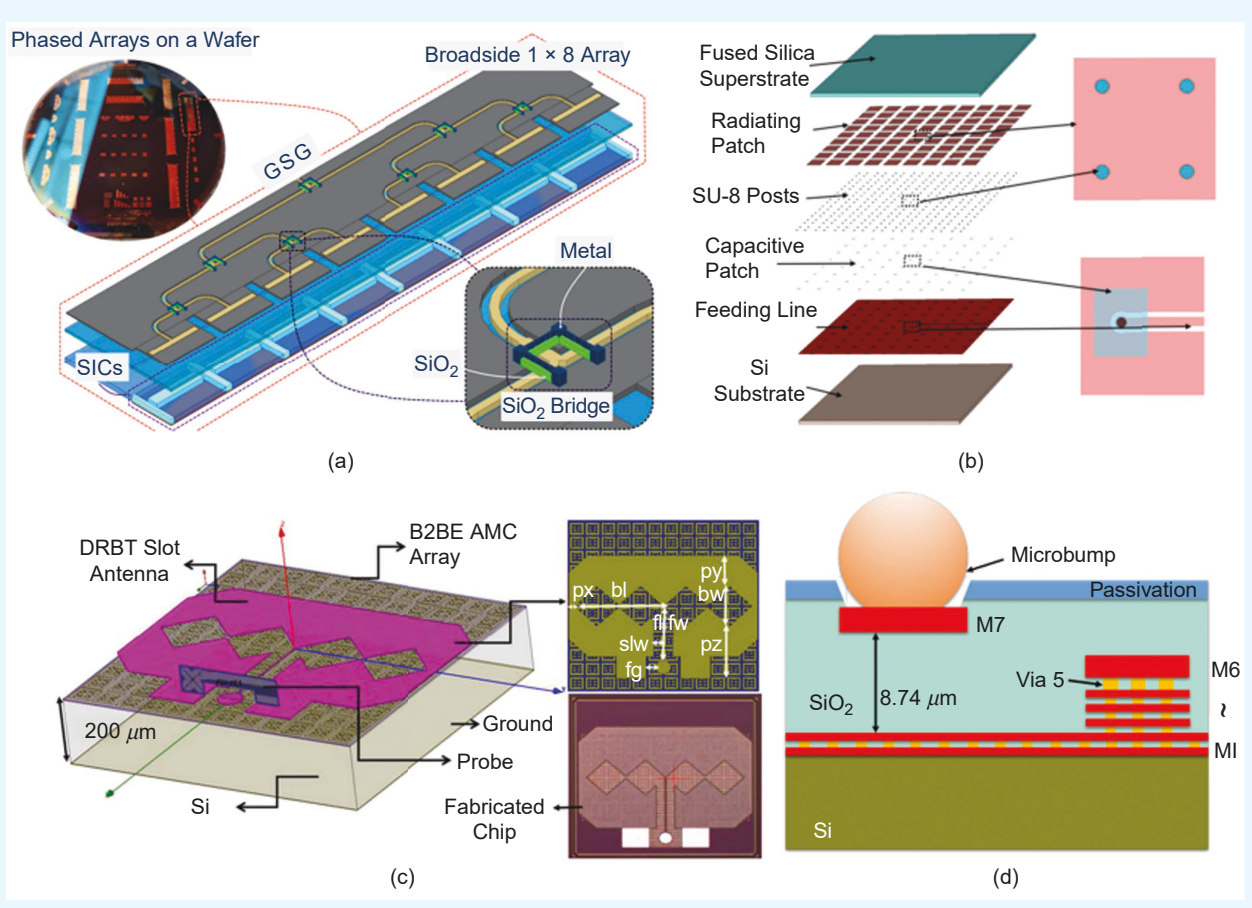

FIGURE 2. Examples of different AoCs. (a) One by eight folded slot arrays with air cavity [13]. (b) An 8 × 8 array with fused silica superstrates [37]. (c) A single-element slot antenna with electromagnetic bandgap structures [14]. (d) A microbump antenna operating at 300 GHz [43]. SIC: silicon-integrated air cavities; GSG: ground-signal-ground; DRBT: double-rhomboid bowtie; B2BE: back-to-back E-shaped; AMC: artificial magnetic conductor.

antennas within a package that contains highly integrated mm-wave radios. In later sections, we discuss emerging technologies for high-speed mm-wave applications such as glass and fan-out processes that go beyond Si and multilayer printed circuit board (PCB) approaches.

GLASS-BASED ANTENNA SOLUTIONS

MM-WAVE ANTENNAS USING A GLASS INTERPOSER

In 2023, Intel announced glass substrates for next-generation advanced packaging. Other companies, such as Absolics, LG Innotek, and Samsung Electro-mechanics in Korea and Dai Nippon Printing and Ibiden in Japan, have all entered the glass substrate market. SKC subsidiary Absolics completed its first glass substrate plant in Covington, GA, USA. The interest in glass substrates is driven by the growing demand for high-performance artificial intelligence (AI) and server semiconductors. As listed in Table 1, glass offers advantages in surface roughness and CTE over organic-core substrates and is more cost-effective with lower capital investment risk than Si substrates. It also reduces packaging height when used as a glass-core substrate. These benefits make glass substrates a promising option for AiP solutions in 5G mm-wave or 6G THz communications.

A research group at the Georgia Institute of Technology (Georgia Tech) has been pioneering the development of mm-wave technology on glass-core substrates [25], [45], [46], [47], [48], [49], [50], [51]. Rehman et al. [25] conducted the first broadband characterization of the electrical properties of Ajinomoto build-up films (ABFs) laminated on glass substrates, characterizing the ABF/glass/ABF stack-up from 20 to 170 GHz [Figure 3(a)]. The authors measured the average insertion loss (IL) of the microstrips to be between 0.12 and 0.62 dB/mm. Lin et al. [45] proposed an endfire antenna based on a monopole tapered radiator using a glass packaging fabrication process, operating from 24 to 40 GHz [Figure 3(b)]. The proposed antenna's single element achieved a measured gain of more than 4 dBi, while the 2 × 1 array demonstrated a gain of more than 6.2 dBi across the entire band.

Erdogan et al. [47] presented a miniaturized D-band quasi-Yagi antenna integrated on a glass interposer. Single-element, 1 × 2, and 1 × 4 arrays were fabricated on 100-µm glass substrates with low-loss polymer films [Figure 3(c)]. The antennas spanned 110–170 GHz and achieved gains of 4.8, 8.4, and 11 dBi for the single-element, 1 × 2, and 1 × 4 arrays, respectively. Jia et al. [48] presented an antenna-integrated glass interposer for D-band 6G wireless applications using die embedding technology [Figure 3(d)]. The authors characterized micro via interconnects in D-band frequencies for chip-to-package interconnects in glass-panel-embedded packages, achieving an average chip-to-package loss of 0.146 dB in the D band and a maximum loss of 0.177 dB at 170 GHz, which is lower than the loss observed in current flip-chip methods. The authors achieved low-loss die-to-package transitions with staggered dielectric vias, showing less than a 0.2-dB IL per transition at 140 GHz. The antenna without the embedded die has an 11.6-dBi broadside gain, while with the embedded die, it has a 10.7-dBi gain at 138 GHz.

Glass interposers are being investigated for AiP solutions, including glass embedding of RFIC chips or passive *RLC* devices. In addition, multidisciplinary studies are needed on the reliability of post through-glass via manufacturing and efficient heat dissipation in glass-embedded devices.

ANTENNA ON DISPLAY

AiP and AoC technologies have been resolving challenges related to bandwidth, gain, polarization, and beam direction by integrating various antenna types and technologies within their multilayered structure. However, the space constraints of today's mobile devices still require a low-cost, multifunction antenna that maximizes coverage at acceptable power levels.

TABLE 1. QUANTITATIVE AND QUALITATIVE COMPARISON OF GLASS VERSUS OTHER PRIMARY SUBSTRATE USED FOR MMWAVE APPLICATIONS.

		Organic		Inorganic	
Substrate Core	**Crystalline Si**	**Laminates**	**Fan out (mold)**	**Ceramic**	**Glass**
Surface roughness (nm)	<10	100–600	40–100	100–500	<10
CTE (ppm/K)	2.3	15–45	16–30	5–7	3–9
Young's modulus (GPa)	130 (100)–169 (110)	10–40	15–25	120–150	45–95
Moisture absorption (%)	0	0.15	1–2.5	0.1	0
Thermal conductivity (W/m·K)	156	0.4	0.5–1	2–4	1.1
Line width/space (µm)	1/1	100/100	5/5	80/80	2/2
Via diameter/pitch (µm)	TSV (10/20)	100/300	25/50	100/300	TGV* (150/300)
Number of layers	10**	30	8	40	4**
Cost	High	Low	High	High	Moderate
Supply chain readiness	Good	Good	Preliminary	Moderate	Moderate

*Laser via. **Number of dielectric layers on the substrate. TGV: through-glass via.

Thus, the development of the AoD concept in mm-wave 5G technology is highly attractive for mm-wave applications.

Before the concept of AoD was introduced, in 2017, Hong et al. [52] first proposed using the transparent region of high-resolution organic light emitting diodes (OLEDs) touch displays to create antennas invisible to the human eye. The authors integrated a transverse magnetic resonant mode antenna within the display, utilizing conductive wire mesh polymer patterns that are composed of the antenna topology. This design maintained optical invisibility while achieving a remarkably high radiation efficiency of 40% and a 1.73-dBi gain. A research group from Pohang University of Science and Technology (POSTECH), led by Hong, was the first to propose [53] and demonstrate [27], [54] AoD technology for mm-wave applications. The AoD concept offers front-side coverage using optically invisible antenna electrodes and packaging technology compatible with current OLED display panels. These approaches involve fabricating the antenna on a distinct transparent film and mounting it either on the uppermost cover window or between the cover window and the metallic display panel (OLED). AoD provides full front-side beam coverage using optically invisible antenna electrodes and packaging technology compatible with modern OLED displays. In addition, flexible PCBs are used in AoD configurations to connect the AoD to the carrier board, providing mechanical flexibility and electrical interconnection [55]. This enables the integration of RF circuits and components within compact designs by mounting the antenna on a transparent film, either on the uppermost cover window or between the cover window and the metallic OLED panel.

In Figure 4(a), the devised diamond-grid-shaped 200 nm-thick Ag-alloy electrodes on glass substrates featured electrical loss characteristics of approximately 0.4 dB/mm at 28 GHz with 88% optical transparency. The 1 × 8 optically invisible AoD exhibited 6.66-dBi boresight gain at 28 GHz while maintaining 88% optical transparency [27]. It achieved a ±60° scanning angle in the *H*-plane, making it highly effective for mm-wave applications. The hybrid electromagnetic sensor (HEMS) was reported to serve both as an antenna and a high-resolution touchscreen display [54]. The fabricated HEMS prototype exhibited flexibility, optical invisibility with over 88% transmittance, and multifunctionality, including an antenna gain of 2.48 dBi (for a two-element array), a –10-dB impedance bandwidth of 1.53 GHz centered at 27.93 GHz, a beam scanning range of ±40°, and a mutual capacitance change ratio that exceeded 4.42%.

Although the process is well developed and shows potential for enhancing the beam coverage of mm-wave devices, AoD technology still needs substantial advancements in bandwidth and polarization agility before it can be fully commercialized. A research group from Ulsan National Institute of Science and Technolog (UNIST) [56] explored an optically invisible artificial magnetic conductor subarray concept to enhance the bandwidth of display-integrated antennas in the mm-wave spectrum [Figure 4(b)]. The thin-metal mesh prototype achieved a 10-dB matching bandwidth of 26% at 28 GHz with an average gain of 1.1 dBi, while maintaining 85% optical transparency, demonstrating its effectiveness in broadening the bandwidth of triband antennas. An interesting new AoD schematic achieved

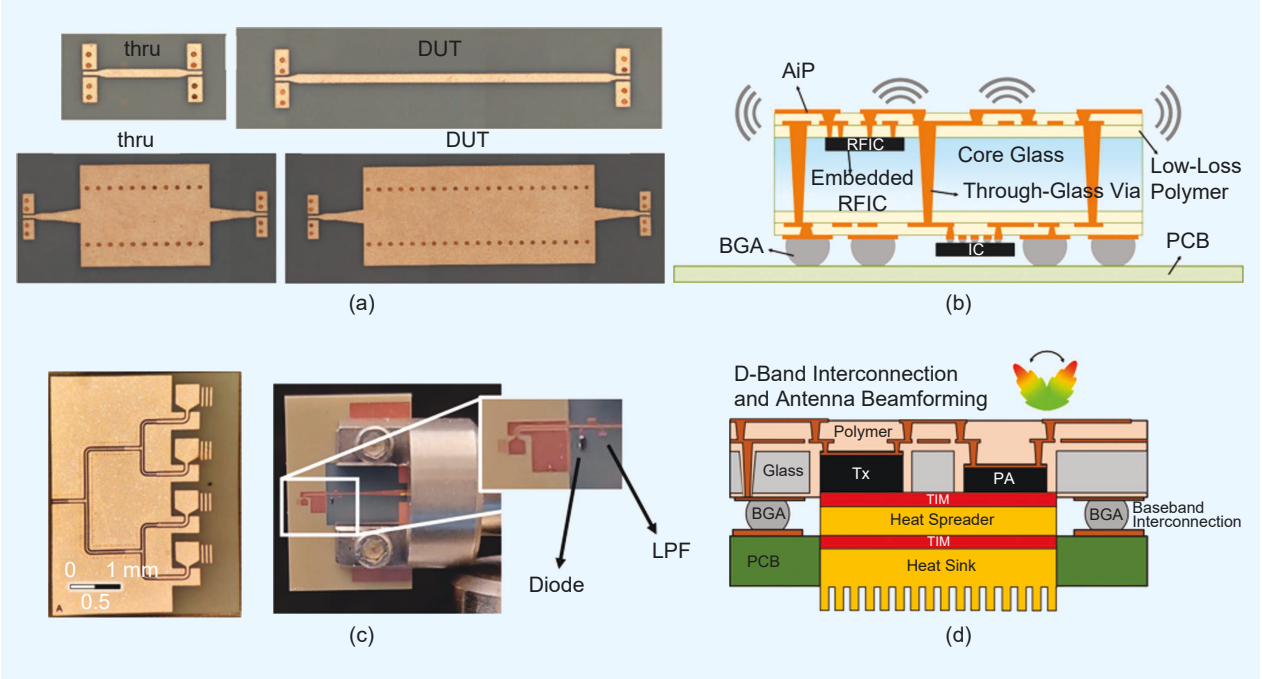

FIGURE 3. Examples of glass substrate devices. (a) ABF/glass/ABF substrate-integrated waveguide (SIW) [25]. (b) An mm-wave endfire antenna [45]. (c) A D-band quasi-Yagi antenna [47]. (d) An antenna-integrated glass interposer for using a die-embedding technique for 6G communication [48]. DUT: device under test; LPF: low-pass filter; BGA: ball-grid array; TIM: thermal interface material; PA: power amplifier; Tx: transmitter.

dual-band operation using a dual-resonance mode (monopole and patch mode) [57] and parasitic structures [58]. Both antenna elements were connected to a differential feed line, ensuring efficient performance across the dual-resonance frequencies [Figure 4(c)]. Transparent electrodes should ensure high electrical conductivity, with metal mesh structures that thus far exceed indium tin oxide, graphene, and polymers [28].

Recent research into glass-based liquid crystal (LC) technologies focuses on leveraging LC's tunability for reconfigurable devices in mm-wave bands [Figure 4(d)] [59], [60]. This approach, which builds on established LCD manufacturing techniques, enables large-area, low-cost fabrication with low power consumption, making it particularly promising for advanced display systems and beam steering antennas. The POSTECH research team proposed the concept of a sustainable reconfigurable intelligent surface for a random wireless propagation channel in mm-wave bands [60].

FUTURE RESEARCH THRUSTS

EMBEDDED WAFER-LEVEL BALL AND FOWLP-BASED AiP

Recently, FOWLP technologies have emerged as promising solutions for small form factors, low-profile packages, higher input–output (I/O) nodes, and enhanced electrical performance. The FOWLP process involves dicing chips from an Si wafer, placing the good die on a carrier wafer, and molding it. A redistribution layer is then created on top of the die and mold area, followed by connecting bumps. This redistributes I/Os to the molding compound outside the die, allowing for more I/O connections than the fan-in wafer-level package. Examples of FOWLP include Infineon's embedded wafer-level ball (eWLB) grid array, Taiwan's Semiconductor Manufacturing Company Limited integrated FOWLP, and Amkor's Si wafer integrated fan-out technology. The FOWLP process first dices the chips, avoiding packaging rejections. The package size is adjustable, making it compatible with existing test infrastructure and flexible solder ball arrangements. It also enables different chips to be mounted in a single package. As a result, several organizations have recently designed antenna systems using FOWLP technology [61] [62] [63].

Yu et al. [64] presented an AiP based on a magnetoelectric (ME) dipole antenna using the FOWLP process, operating at 25–43 GHz [Figure 5(a)]. The authors used vertical Cu interconnects for the ME dipole to achieve dual polarization. The antenna gain was 5 dBi, with the array exceeding 10 dBi over 25–43 GHz. The dipole array provided a scanning range of ±40° with less than 3-dB gain degradation and ±50° with less than 4-dB degradation. This ME dipole antenna has the potential for 5G mm-wave applications such as customer premise equipment and micro base stations. Fischer et al. [65] designed a folded dipole antenna integrated in an eWLB package for 77-GHz automotive radar applications [Figure 5(b)]. The monolithic microwave IC included a 77-GHz signal source and a transceiver with an amplifier and a mixer. The system featured four channels, with the one-channel folded dipole sensor having a maximum gain of 6.2 dBi and the full antenna array (channels 1, 2, 3, and 4) achieving a maximum gain of 8.2 dBi. Lee et al. [66] proposed FOWLP-based AiPs with endfire radiation characteristics at 60–90 GHz [Figure 5(c)]. The authors demonstrated a 1 × 4 asymmetric-fed interdigital coupling antenna (AFICA) array

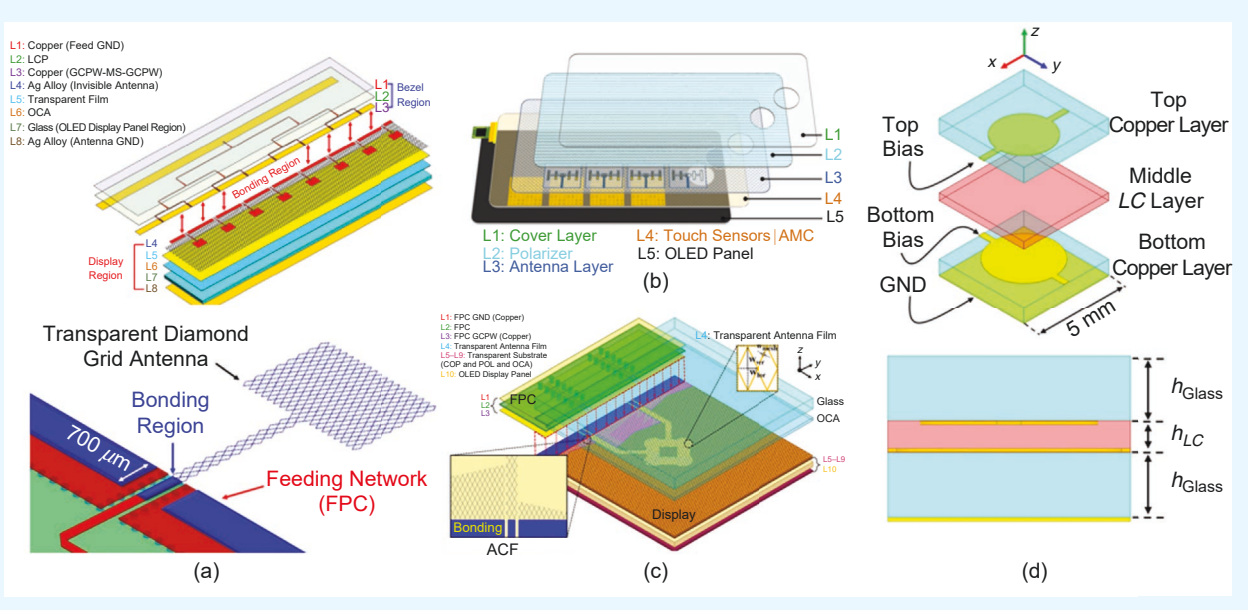

FIGURE 4. Demonstrations of optically invisible antennas. (a) A Pohang University of Science and Technology (POSTECH) 1 × 8 AoD array [27]. (b) UNIST optically invisible artificial magnetic connector subarray with dipole antenna [56]. (c) POSTECH dual-polarized dual-band AoD [57] [58]. (d) POSTECH LCD reconfigurable intelligent surface technology [60]. GND: ground; ACF: anisotropic conductive film; MMIC: monolithic microwave IC; LCP: liquid crystal polymer; OCA: optically clear adhesive; FPC: flexible printed circuit; GCPW: grounded coplanar waveguide; COP: cycloolefin polymer; POL: polarizer.

that achieved more than 80% efficiency with an extremely low profile of $0.044\lambda_0$ at 60 GHz. The proposed package with transmitter module provides a wide scan angle of ±50°, low sidelobe level (≤–10 dB), and low cross-polarization level (≤–18 dB) in the operating band. The frequency quadrupler CMOS chip was integrated with the AFICA array to enable commercial radar and communications applications.

EXOTIC MATERIALS

Exotic materials that alternate between conductive and dielectric states are being investigated for potential use in AiP or AoC technology in the mm-wave band. In particular, PCMs are used in mm-wave reconfigurable systems due to their tunable properties such as electrical resistance and optical transmittance. VO_2 is unique among PCMs for its ability to undergo a reversible solid-to-solid phase transition at a low temperature of 68 °C [67]. Unlike other PCMs such as germanium antimony telluride (GST) or germanium telluride (GeTe), which require high temperatures (618 °C or 725 °C) to switch between conductive and dielectric states, the low transition temperature of VO_2 makes excitation easier to implement. VO_2 functions as an insulator (1–10 MΩ/sq) below 68 °C, but transitions to a conductor (10–100 Ω/sq) above this threshold. This dramatic change in conductivity is due to the response of the VO_2 crystal structure to temperature, strain, or electric field. Below 68 °C, VO_2 has a monoclinic structure, which transitions to a rutile structure as the temperature rises [68]. In general, the insulator-metal transition of VO_2 changes its resistivity by a factor of three to four. VO_2 exhibits low-loss RF characteristics at mm-wave frequencies, unlike lossy semiconductor-based transmission lines such as p-i-n diodes or CMOS switches [30]. In addition, VO_2's intrinsic transition time is in the order of nanoseconds or less [69].

A research team at Georgia Tech has developed VO_2-integrated passive devices with low-loss reconfigurable RF characteristics. Chen et al. [33] investigated the performance and reliability of VO_2 thin-film shunt switches integrated with coplanar waveguides (CPWs) in the 35–45-GHz range. The switch transitioned between the dielectric and conductive states of VO_2 using two parallel Joule heaters. After 100 million thermal cycles, the electrical properties of the VO_2 switch remained stable. Moreover, West

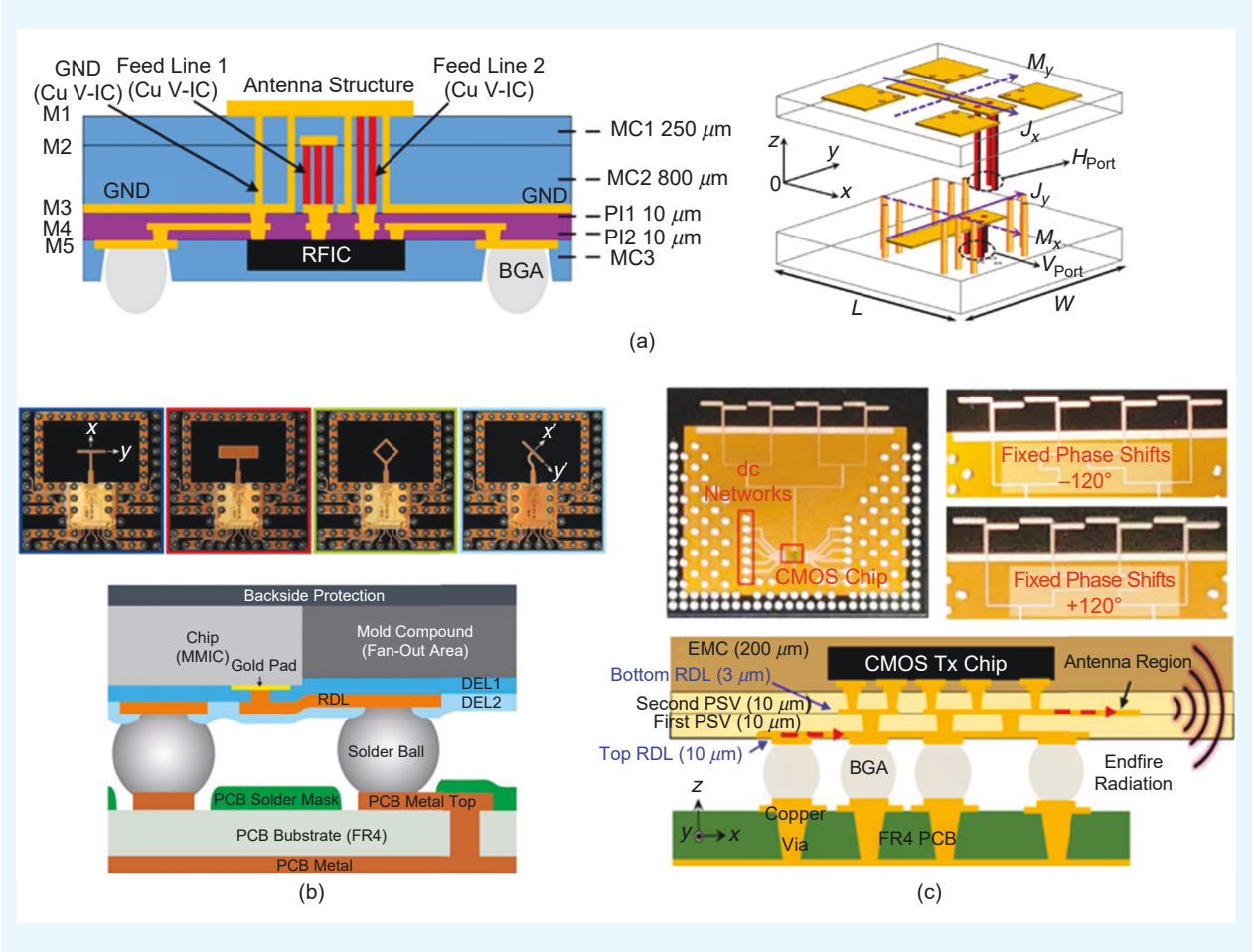

FIGURE 5. Demonstrations of FOWLP-based AiP. (a) Wideband ME dipole AiP with vertical Cu interconnects [64], (b) folded dipole antenna package for 77 GHz automotive radar [65], and (c) endfire antenna at 60—90 GHz with integrated frequency quadrupler CMOS chip [66]. FR4: flame retardant 4; ME: magnetoelectric; RDL: redistribution layer; PSV: passivation.

et al. [30] proposed a photothermally excited VO_2 RF switch operating from dc to 65 GHz [Figure 6(a)]. The CPW switches exhibited low-loss, ultrawideband performance with a <0.43-dB insertion loss (IL) and > 17.7-dB return loss in the ON state, and > 17.2-dB isolation in the OFF state from 10 MHz to 65 GHz.

Lust et al. [32] proposed a packaged reconfigurable dual-sense linear-to-circular-polarization converter using a VO_2-based metasurface in the Ka-band (27.5–31 GHz). The device featured a four-layer metasurface 90° with rotational symmetry for right-hand circular polarization and left-hand circular polarization (LHCP) conversion. The measured results for LHCP conversion showed an axial ratio ≤2.1 dB and IL ≤4 dB, with a 1-dB axial ratio at 30.2–32.4 GHz. The polarizer was packaged on a PCB for dc biasing, with each VO_2 metasurface placed on the PCB using a flip-chip bonder [Figure 6(b)]. This entire packaging process for the VO_2 polarizer highlights the potential of VO_2 for future AiP applications. Yang et al. [70] proposed a frequency-reconfigurable filter that covers multiple bands, reducing cost and size at the system level. Notably, the VO_2 in this study was not created through microfabrication but printed using custom inks. The authors demonstrated a fully printed, frequency-reconfigurable bandpass filter on a flexible polyimide (PI) substrate that switches from 4 to 3.7 GHz using a dual-mode resonator, as illustrated in Figure 6(c). A flexible reconfigurable filter has the potential to be designed in the mm-wave band using a low-loss flexible substrate.

In summary, reconfigurable devices, including filters or switches, can be designed with low mm-wave losses. Such devices can be fabricated through a microfabrication process or inkjet printing using novel PCMs such as VO_2. VO_2 can potentially be integrated into AoCs or multilayer AiPs, offering exciting future mm-wave applications depending on its fabrication method. Other exotic materials, for example, GeTe [71], SiC [21], graphene [72], and paraffin [35], can alter or affect the conductive or dielectric properties of antennas.

TOWARD A 3D ANTENNA AND ITS PACKAGING STRUCTURE

AI solutions require rapid computation and storage of massive numbers of data. High-bandwidth memory (HBM), introduced in 2013, is a high-speed memory interface based on 3D stacked memory technology. It connects to CPUs or GPUs for fast data transfers, making it ideal for applications such as high-resolution graphics, data centers, AI, and machine learning. HBM has been the leading memory solution in the AI market, optimized for high performance with high speed and capacity via TSV-based stacking. TSV technology is used to transfer data vertically through memory layers, reducing interconnect distances and significantly increasing bandwidth.

3D stacking has been little explored from an antenna perspective [73], [74], [75]. Jin et al. [73] proposed an

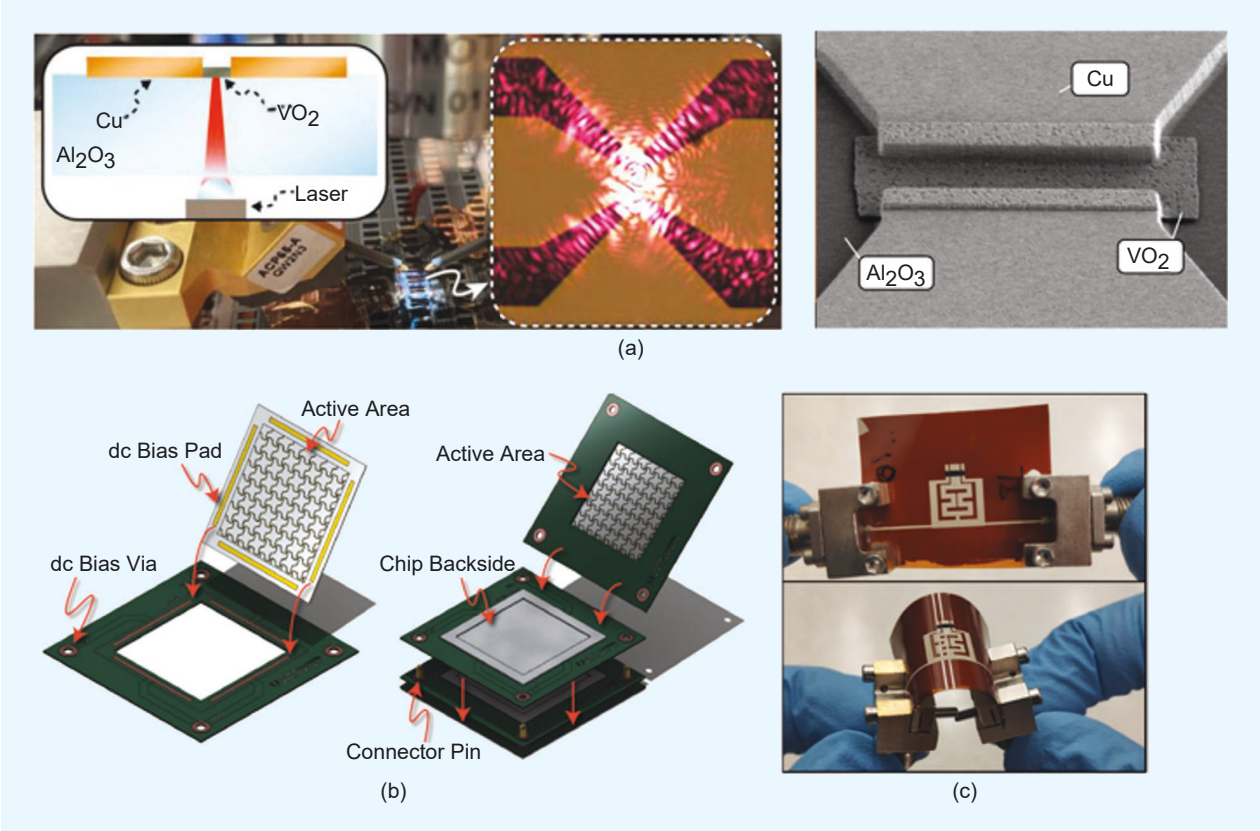

FIGURE 6. (a) Micrographs of the VO_2-based CPW switch [30]. (b) VO_2-based polarizer and assembly process [32]. (c) Fabricated VO_2 filter in flat and bent states [70].

aperture-coupled AiP on high-resistance Si (HRSi) substrates using wafer-level packaging (WLP) technology with TSV interconnects [Figure 7(a)]. The designed antenna consisted of two stacked high-HRSi substrates: a 750-μm-thick lower substrate with a slot radiator and CPW feed, and a 200-μm-thick upper substrate with patches to enhance gain and efficiency. Vertical interconnects using TSVs were incorporated to carry RF signals up to the mm-wave band. The measured results showed broadband radiation with a gain of 2.4 dBi from 76 to 93 GHz. Interestingly, this WLP platform can also support embedded passives, saving die area by moving on-chip passives into the package.

In addition to Si-to-Si vertical interconnections, Malta et al. [74] demonstrated that glass interposers can be stacked with SiGe beamformers [Figure 7(b)]. The authors presented a 3D heterogeneous integration of RF tiles for a multifunctional airborne sensor system, including a W-band active electronically scanned array radar. Each phased-array tile contained a high-speed SiGe BiCMOS beamformer chip vertically integrated via TSVs on a glass substrate with an RF interposer and a patch antenna array. The integration concept is illustrated in Figure 15(b). The tiles, each with multiple elements, were combined into subarrays on a single board, which were then assembled into larger arrays. The tile approach used TSVs to route dc power, ground, logic commands, and RF (intermediate frequency/local oscillator) signals from the subarray board through the SiGe layer to the glass interposer. Tang et al. [24] proposed the use of TSVs in an on-chip antenna structure, specifically for a 300-GHz aperture antenna in InP technology for THz transceivers, as illustrated in Figure 7(c). The authors used TSVs to create quasi-substrate-integrated waveguide (SIW) cavities that ensure robust antenna performance despite varying chip sizes in ICs. In addition, a dual-mode aperture antenna was proposed with quasi-SIW cavities that enable higher-order modes to increase impedance bandwidth. The radiation pattern of the even TM_{120} mode was reconstructed by the radiation aperture, achieving a gain of 8 dBi.

Studies of 3D antennas that use TSVs across different frequencies and technologies, such as AiP and WLP, demonstrate their advantages in scalable arrays but at the cost of increased process complexity. For monolithically integrated AoCs in high data rate applications, TSVs can also reduce losses by eliminating the need for wire bonding [76]. In addition, research is ongoing to address the thermal reliability [77] and mechanical reliability [78] of TSVs. Dimensions of TSVs should also minimize their impact on impedance matching. Organic materials can be used as interposers, in addition to Si interposers using

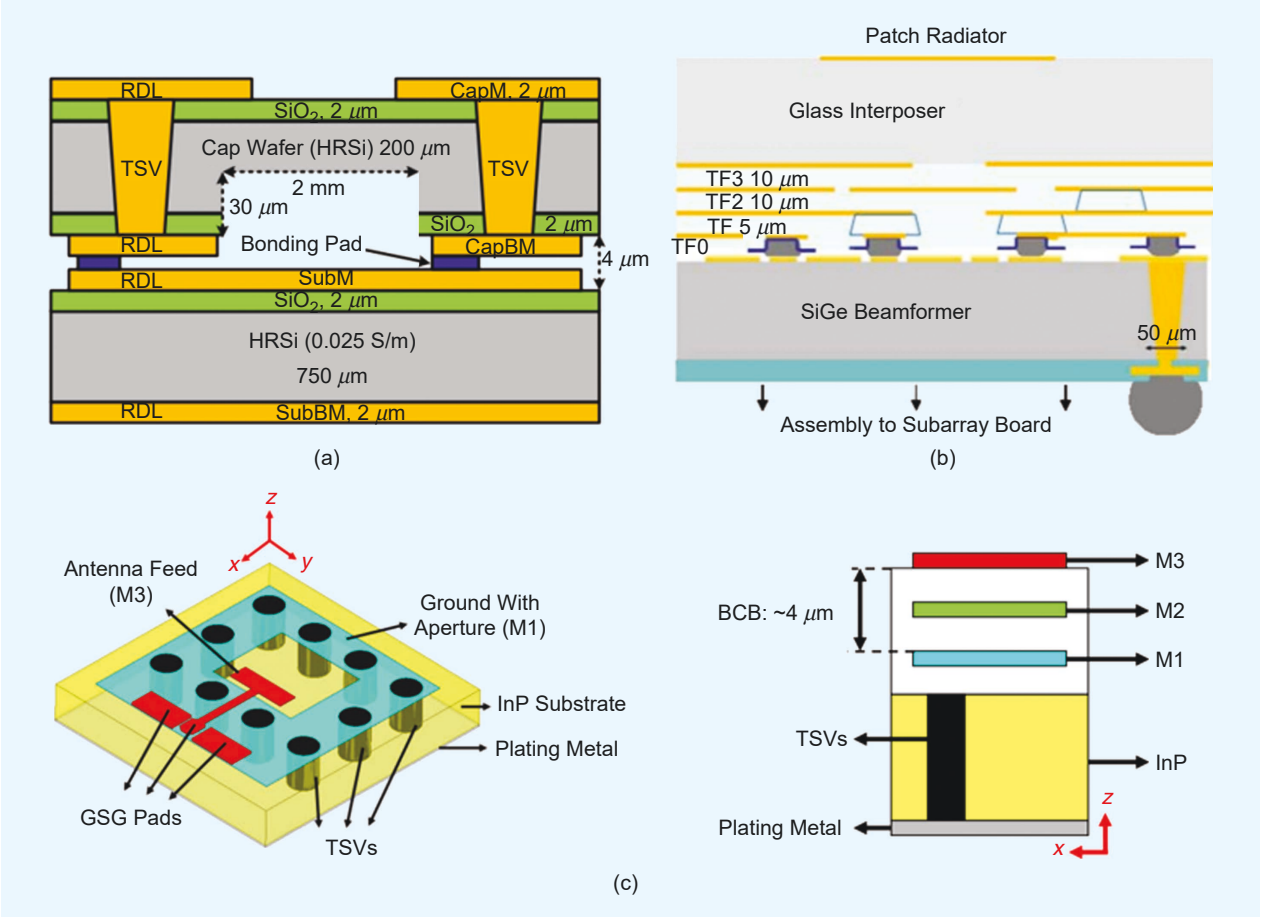

FIGURE 7. Cross-sectional views of (a) the proposed 3D AiP module with TSV interconnection [73], (b) 3D-integrated phased-array tile using a glass interposer and SiGe beamformer [74], and (c) 0.7-μm InP process and 3D geometry of the on-chip antenna with TSVs [24]. BCB: benzocyclobutene.

TSVs. Further research is needed to optimize vertical interconnects for antennas and transmission lines [79], [80], [81].

MM-WAVE 5G AND BEYOND: KEY TAKEAWAYS

6G targets characteristics such as 10× faster data rates, 1/10th less latency, and 10× better connectivity than 5G. Although 6G upper-middle and D-band research is ongoing, the 5G mm-wave market is still in its early stages, awaiting implementation across various applications such as virtual reality, augmented reality, metaverse platforms, and biomedical devices. We summarize the two-part article and discuss how each applies to mm-wave antenna development, as illustrated in Figure 8.

Selecting the proper frequency is key to ensuring sufficient bandwidth and aligns closely with the needs of the application, such as 28/39 GHz for 5G phased arrays, or 77 GHz for automotive radar systems. To reduce the risk of failure, one may periodically monitor the standards organizations' (e.g., the International Telecommunication Union, 3rd Generation Partnership Project, and IEEE) documents on spectrum allocation and conduct research aligned with intended spectrum use. In the 2G/3G/4G era, antennas were placed on PCBs, but now, antennas are increasingly being integrated into the same package with other microwave components. We have explored various mm-wave packaged antenna structures including AiPs, AoCs, glass-based AiPs, AoDs, FOWLP-based AiPs, and 3D AiPs. For multilayer AiP, an ME dipole antenna [82] with an identical 3-dB beamwidth in the *E*-/*H*-plane, or a patch antenna [83] with easy dual-polarization implementation is advantageous. Dipoles or slots [17] can be used in AoC designs for RF front ends that require differential characteristics. Patch [37] or folded slots [13] are also promising antennas for AoCs that provide broadside radiation characteristics and a compact footprint. By calculating the link budget, effective isotropic radiated power and total radiated power are determined in advance, allowing researchers to backtrack and identify the required antenna realized gain and efficiency for development. We have categorized multilayer organic laminates, low-temperature co-fired ceramic (LTCC), Si, and glass materials and highlighted their advantages and disadvantages. Electrical/mechanical/thermal data should be carefully collected, analyzed, and compared prior to design and integration.

Choosing the right substrate involves factors like permittivity, loss tangent, CTE, Young's modulus, T_g, moisture absorption, and thermal conductivity. In addition, flame retardant 4 (FR4) process compatibility should also be evaluated for reduced cost manufacturing. Material selection is tied to design rules and manufacturability, including the number of layers, line/space features, and via radius/space. As permittivity and loss tangent are key factors that determine antenna footprint and radiation efficiency, thorough characterization is required at the frequency of interest using methods such as the ring resonator method. If a complex, less-reliable process such as TSV is chosen, it should offer advantages over laminating processes, such as improved heat dissipation using Si's high thermal conductivity. 2.5D and 3D heterogeneous integration using TSV and hybrid bonding provide compact package sizes, making them attractive candidates for mobile devices. The works in [2] and [84] are valuable resources that provide guidelines for various antenna functionalities such as analog/digital/hybrid beamforming; multiple-input, multiple-output; multibeams; and reconfigurable antennas.

Cost-effectiveness is important to the development of mm-wave antenna technology for high-performance communication systems. To be affordable, costs should be reduced through manufacturing optimization, supply chain improvement, lower material costs, increased die yield, and panel/wafer scaling. Reducing costs, especially by utilizing FR4-compatible or hybrid processes, will also need to be explored. This is a key area that requires continued attention from industry. We highlight general and novel packaging processes, from flip-chip to hybrid bonding, to achieve high gain and low-loss characteristics within the link budget. Smooth surface roughness is critical for low-loss interconnects. Addressing electromagnetic compatibility, signal integrity, and power integrity are needed to secure the performance of surrounding analog, digital, and RF ICs. Ensuring reliability through efficient heat dissipation is important, but beyond the scope of this article. Efforts should focus on achieving both optimal thermal and electrical performance through integrated electrical and thermal co-design.

FIGURE 8. Guidelines for developing antennas in the mm-wave band. NR: New Radio; BW: bandwidth; EIRP: effective isotropic radiated power; TRP: total radiated power; PPE: polyphenylene ether; HBT: heterojunction bipolar transistor; MIMO: multiple-input, multiple-output; freq.: frequency; satcom: satellite communications; EMI: electromagnetic interference; PI: power integrity; SI: signal integrity; IoT: Internet of Things; LRR: long-range radar; SRR: short-range radar; PTFE: polytetrafluoroethylene; BT: bismaleimide triazine; LP: linear polarization; CP: circular polarization; DP: dual polarization; HDI: high-density interconnect; Recon.: reconfigurability; Comm.: communication.

CONCLUSION

This two-part article aimed to spark interest and provide in-depth insights into the latest advancements in antennas, materials, packaging, and integration technologies. We provided an overview of antennas using different packaging technologies in the mm-wave band. In part 1, we presented the latest AiP research, focusing on material and application aspects, with a discussion on Si-based phased-array systems and integration. Part 2 explored AoC solutions for highly integrated mm-wave devices, new AiP configurations with glass-core substrates for 5G and beyond, and a unique AoD concept for mobile devices. Emerging technologies, including novel materials, FOWLP, and 3D packaging, were also covered. We hope that this article provides the reader with a pathway to explore antenna/package integration.

ACKNOWLEDGMENT

This research was sponsored in part by the U.S. National Science Foundation under Grant 2300156, Grant 2329251, Grant 2149886, Grant 1711102, and Grant 1408228. This work was also supported in part by Institute of Information and Communications Technology Planning and Evaluation grants funded by the Korean government (Grant RS-2024—00354970 and Grant 2021-0-00763) and in part supported by National Research Foundation of Korea (Grant RS-2025—00514623). Seung Yoon Lee and Dongseop Lee contributed equally. Wonbin Hong and Nima Ghalichechian are co-corresponding authors.

AUTHOR INFORMATION

Seung Yoon Lee (seungyoon.lee@gatech.edu) is a Ph.D. candidate in electrical and computer engineering at the School of Electrical and Computer Engineering, Georgia Institute of Technology, Atlanta, GA 30308 USA. His research interests include millimeter-wave on-chip antennas, antenna integration and packaging, and vanadium dioxide phase-change materials. He is a Graduate Student Member of IEEE.

Dongseop Lee (dongseopl@postech.ac.kr) is a Ph.D. student in electrical engineering at the Department of Electrical Engineering, Pohang University of Science and Technology (POSTECH), Seoul 37673, South Korea. His research interests include millimeter-wave 5G radio-frequency front-end modules, antennas on display, antennas in/on package, and antennas on chip. He is a Graduate Student Member of IEEE.

Yueping Zhang (eypzhang@ntu.edu.sg) is a professor of electronic engineering at the School of Electrical and Electronic Engineering, Nanyang Technological University, 639798, Singapore. He has been working actively on radio electronics for decades. He is known for his work on integrated antennas. He is a Fellow of IEEE.

Wonbin Hong (whong@postech.ac.kr) is a distinguished professor at the Department of Electrical Engineering, Pohang University of Science and Technology (POSTECH), Seoul 37673, South Korea. His research interests include antennas, radio-frequency circuits, packaging, and various areas of applied electromagnetics. He is a Fellow of IEEE.

Nima Ghalichechian (nghalich3@gatech.edu) is an associate professor at the School of Electrical and Computer Engineering, Georgia Institute of Technology, Atlanta, GA 30308 USA. He is the director of the mmWave Antennas and Arrays Laboratory. His research interests include millimeter-wave (mmWave) phased arrays, reconfigurable antennas, reflectarrays, transmitarrays, on-chip antennas, phase-change materials, nonreciprocal microwave devices, high-power arrays, and mmWave measurement techniques. He is a Senior Member of IEEE.

REFERENCES

[1] S. Y. Lee, D. Lee, Y. Zhang, W. Hong, and N. Ghalichechian, "History and latest progress in antenna packaging technology. Part 1. Multilayer solutions," *IEEE Antennas Propag. Mag.*, early access, May 1, 2025, doi: 10.1109/MAP.2025.3560852.

[2] W. Hong et al., "The role of millimeter-wave technologies in 5G/6G wireless communications," *IEEE J. Microw.*, vol. 1, no. 1, pp. 101–122, Jan. 2021, doi: 10.1109/JMW.2020.3035541.

[3] D. Liu and Y. P. Zhang, "Integration of array antennas in chip package for 60-GHz radios," *Proc. IEEE*, vol. 100, no. 7, pp. 2364–2371, Jul. 2012, doi: 10.1109/JPROC.2012.2186101.

[4] W. Hong, K. H. Baek, Y. Lee, Y. Kim, and S. T. Ko, "Study and prototyping of practically large-scale mmWave antenna systems for 5G cellular devices," *IEEE Commun. Mag.*, vol. 52, no. 9, pp. 63–69, Sep. 2014, doi: 10.1109/Mcom.2014.6894454.

[5] Y. Zhang and J. Mao, "An overview of the development of antenna-in-package technology for highly integrated wireless devices," *Proc. IEEE*, vol. 107, no. 11, pp. 2265–2280, Nov. 2019, doi: 10.1109/JPROC.2019.2933267.

[6] W. Ruoyu, S. Yaoming, M. Kaynak, S. Beer, J. Borngräber, and J. C. Scheytt, "A micromachined double-dipole antenna for 122 – 140 GHz applications based on a SiGe BiCMOS technology," in *Proc. IEEE/MTT-S Int. Microw. Symp. Dig.*, Jun. 2012, pp. 1–3, doi: 10.1109/MWSYM.2012.6258421.

[7] A. Babakhani, X. Guan, A. Komijani, A. Natarajan, and A. Hajimiri, "A 77-GHz phased-array transceiver with on-chip antennas in silicon: Receiver and antennas," *IEEE J. Solid-State Circuits*, vol. 41, no. 12, pp. 2795–2806, Dec. 2006, doi: 10.1109/JSSC.2006.884811.

[8] D. Hou, Y. Z. Xiong, W. Hong, W. L. Goh, and J. Chen, "Silicon-based on-chip antenna design for millimeter-wave/THz applications," in *Proc. IEEE Elect. Des. Adv. Packag. Syst. Symp. (EDAPS)*, 2011, pp. 1–4, doi: 10.1109/EDAPS.2011.6213767.

[9] H. Zhang and A. Shamim, "Gain enhancement of millimeter-wave on-chip antenna through an additively manufactured functional package," *IEEE Trans. Antennas Propag.*, vol. 68, no. 6, pp. 4344–4353, Jun. 2020, doi: 10.1109/TAP.2020.2975276.

[10] E. Ojefors, K. Grenier, L. Mazenq, F. Bouchriha, A. Rydberg, and R. Plana, "Micromachined inverted F antenna for integration on low resistivity silicon substrates," *IEEE Microw. Wireless Compon. Lett.*, vol. 15, no. 10, pp. 627–629, Oct. 2005, doi: 10.1109/LMWC.2005.856693.

[11] W. T. Khan et al., "A D-band micromachined end-fire antenna in 130-nm SiGe BiCMOS technology," *IEEE Trans. Antennas Propag.*, vol. 63, no. 6, pp. 2449–2459, Jun. 2015, doi: 10.1109/TAP.2015.2416751.

[12] S. Pan and F. Capolino, "Design of a CMOS on-chip slot antenna with extremely flat cavity at 140 GHz," *IEEE Antennas Wireless Propag. Lett.*, vol. 10, pp. 827–830, 2011, doi: 10.1109/LAWP.2011.2163291.

[13] S. Y. Lee, D. L. West, S. A. Dasari, and N. Ghalichechian, "On-chip miniaturized cavity V-band coplanar folded slot array with high efficiency and reduced mutual coupling," *IEEE Trans. Antennas Propag.*, vol. 72, no. 9, pp. 7317–7322, Sep. 2024, doi: 10.1109/TAP.2024.3424554.

[14] M. S. Khan, F. A. Tahir, A. Meredov, A. Shamim, and H. M. Cheema, "A W-band EBG-backed double-rhomboid bowtie-slot on-chip antenna," *IEEE Antennas Wireless Propag. Lett.*, vol. 18, no. 5, pp. 1046–1050, May 2019, doi: 10.1109/LAWP.2019.2908891.

[15] J. M. Edwards and G. M. Rebeiz, "High-efficiency elliptical slot antennas with quartz superstrates for silicon RFICs," *IEEE Trans. Antennas Propag.*, vol. 60, no. 11, pp. 5010–5020, Nov. 2012, doi: 10.1109/TAP.2012.2207353.

[16] H. Chu, Y. X. Guo, T. G. Lim, Y. M. Khoo, and X. Q. Shi, "135-GHz micromachined on-chip antenna and antenna array," *IEEE Trans. Antennas Propag.*, vol. 60, no. 10, pp. 4582–4588, Oct. 2012, doi: 10.1109/Tap.2012.2209855.

[17] Y. C. Ou and G. M. Rebeiz, "Differential microstrip and slot-ring antennas for millimeter-wave silicon systems," *IEEE Trans. Antennas Propag.*, vol. 60, no. 6, pp. 2611–2619, Jun. 2012, doi: 10.1109/Tap.2012.2194651.

[18] Y. P. Zhang and D. Liu, "Antenna-on-chip and antenna-in-package solutions to highly integrated millimeter-wave devices for wireless communications," *IEEE Trans. Antennas Propag.*, vol. 57, no. 10, pp. 2830–2841, Oct. 2009, doi: 10.1109/TAP.2009.2029295.
[19] P. Burasa, T. Djerafi, N. G. Constantin, and K. Wu, "On-chip dual-band rectangular slot antenna for single-chip millimeter-wave identification tag in standard CMOS technology," *IEEE Trans. Antennas Propag.*, vol. 65, no. 8, pp. 3858–3868, Aug. 2017, doi: 10.1109/TAP.2017.2710215.
[20] T. Karacolak, R. V. K. G. Thirumalai, J. N. Merrett, Y. Koshka, and E. Topsakal, "Silicon carbide (SiC) antennas for high-temperature and high-power applications," *IEEE Antennas Wireless Propag. Lett.*, vol. 12, pp. 409–412, 2013, doi: 10.1109/LAWP.2013.2251599.
[21] S. A. Dasari, S. Y. Lee, and N. Ghalichechian, "Towards harsh environment silicon carbide based on-chip antenna," in *Proc. United States Nat. Committee URSI Nat. Radio Sci. Meeting (USNC-URSI NRSM)*, 2025, pp. 18–19, doi: 10.23919/USNC-URSINRSM66067.2025.10907226.
[22] I. S. Chen, H. K. Chiou, and N. W. Chen, "V-band on-chip dipole-based antenna," *IEEE Trans. Antennas Propag.*, vol. 57, no. 10, pp. 2853–2861, Oct. 2009, doi: 10.1109/TAP.2009.2031758.
[23] L. Ohlsson et al., "Slot-coupled millimeter-wave dielectric resonator antenna for high-efficiency monolithic integration," *IEEE Trans. Antennas Propag.*, vol. 61, no. 4, pp. 1599–1607, Apr. 2013, doi: 10.1109/TAP.2012.2237005.
[24] S. Y. Tang et al., "Terahertz on-chip aperture antenna with through substrate vias for enhanced gain and chip-size insensitivity in InP technology," *IEEE Trans. Antennas Propag.*, vol. 71, no. 9, pp. 7184–7195, Sep. 2023, doi: 10.1109/TAP.2023.3292502.
[25] M. u. Rehman, S. Ravichandran, A. O. Watanabe, S. Erdogan, and M. Swaminathan, "Characterization of ABF/glass/ABF substrates for mmWave applications," *IEEE Trans. Compon. Packag. Manuf. Technol.*, vol. 11, no. 3, pp. 384–394, Mar. 2021, doi: 10.1109/TCPMT.2021.3061485.
[26] M. u Rehman, L. N. V. Kumar, and M. Swaminathan, "Characterization of microstrip line and SIW on ABF in glass interposers for mmWave applications," *IEEE Trans. Compon. Packag. Manuf. Technol.*, vol. 13, no. 9, pp. 1520–1523, Sep. 2023, doi: 10.1109/TCPMT.2023.3305459.
[27] J. Park, S. Y. Lee, J. Kim, D. Park, W. Choi, and W. Hong, "An optically invisible antenna-on-display concept for millimeter-wave 5G cellular devices," *IEEE Trans. Antennas Propag.*, vol. 67, no. 5, pp. 2942–2952, May 2019, doi: 10.1109/TAP.2019.2900399.
[28] S. Y. Lee, M. Choo, S. Jung, and W. Hong, "Optically transparent nanopatterned antennas: A review and future directions," *Appl. Sci.*, vol. 8, no. 6, p. 901, 2018.
[29] J. D. Cressler and G. Niu, *Silicon-Germanium Heterojunction Bipolar Transistors*. Boston, MA, USA: Artech House, 2003.
[30] D. L. West, A. A. Goodnight, and N. Ghalichechian, "Ultrawideband, photothermally excited mmWave vanadium dioxide switches," *IEEE Microw. Wireless Technol. Lett.*, vol. 34, no. 9, pp. 1083–1086, Sep. 2024, doi: 10.1109/LMWT.2024.3422848.
[31] J. A. Ramsey, S. Y. Lee, W. R. Disharoon, D. L. West, and N. Ghalichechian, "Low-loss vanadium dioxide-enabled mmWave tunable reflective electromagnetic surface with complementary unit cells for wave manipulation," *J. Appl. Phys.*, vol. 135, no. 21, Jun. 2024, Art. no. 214901, doi: 10.1063/5.0211712.
[32] M. S. Lust, D. L. West, V. Smet, T. G. Williamson, and N. Ghalichechian, "Vanadium-dioxide-based reconfigurable Ka-band dual-sense linear-to-circular polarizer," *IEEE Trans. Antennas Propag.*, vol. 72, no. 3, pp. 2468–2480, Mar. 2024, doi: 10.1109/TAP.2024.3356615.
[33] S. Chen, M. Lust, A. Roo, and N. Ghalichechian, "Reliability of VO_2-based mmWave switches under 100 million thermal cycles," *IEEE Trans. Device Mater. Rel.*, vol. 23, no. 2, pp. 241–248, Jun. 2023, doi: 10.1109/TDMR.2023.3249771.
[34] B. Ghassemiparvin and N. Ghalichechian, "Paraffin-based reconfigurable antenna operating at 100 GHz," *J. Microelectromech. Syst.*, vol. 29, no. 5, pp. 621–628, Oct. 2020, doi: 10.1109/JMEMS.2020.3013159.
[35] B. Ghassemiparvin and N. Ghalichechian, "Paraffin-based RF microsystems for millimeter-wave reconfigurable antenna," *IEEE Trans. Antennas Propag.*, vol. 70, no. 1, pp. 744–749, Jan. 2022, doi: 10.1109/TAP.2021.3102112.
[36] Y. S. Huang, L. Zhou, J. F. Mao, and Q. Xu, "A W-band high radiation efficiency with BCB-air cavity-backed antenna based on through silicon ring trench," *IEEE Antennas Wireless Propag. Lett.*, vol. 21, no. 10, pp. 1955–1959, Oct. 2022, doi: 10.1109/LAWP.2022.3186917.
[37] J. Li, C. Matos, S. Chen, and N. Ghalichechian, "Fundamental improvement to the efficiency of on-chip mmWave phased arrays using MEMS suspension," *IEEE Antennas Wireless Propag. Lett.*, vol. 20, no. 4, pp. 473–477, Apr. 2021, doi: 10.1109/LAWP.2021.3054555.
[38] S. Zihir, O. D. Gurus, A. Kar-Roy, S. Raman, and G. M. Rebeiz, "60-GHz 64- and 256-elements wafer-scale phased-array transmitters using full-reticle and subreticle stitching techniques," *IEEE Trans. Microw. Theory Techn.*, vol. 64, no. 12, pp. 4701–4719, Dec. 2016, doi: 10.1109/TMTT.2016.2623948.
[39] M. R. Nezhad-Ahmadi, M. Fakharzadeh, B. Biglarbegian, and S. Safavi-Naeini, "High-efficiency on-chip dielectric resonator antenna for mm-Wave transceivers," *IEEE Trans. Antennas Propag.*, vol. 58, no. 10, pp. 3388–3392, Oct. 2010, doi: 10.1109/TAP.2010.2055802.
[40] P. V. Bijumon, Y. M. M. Antar, A. P. Freundorfer, and M. Sayer, "Dielectric resonator antenna on silicon substrate for system on-chip applications," *IEEE Trans. Antennas Propag.*, vol. 56, no. 11, pp. 3404–3410, Nov. 2008, doi: 10.1109/TAP.2008.2005537.
[41] S. Pan, F. Caster, P. Heydari, and F. Capolino, "A 94-GHz extremely thin metasurface-based BiCMOS on-chip antenna," *IEEE Trans. Antennas Propag.*, vol. 62, no. 9, pp. 4439–4451, Sep. 2014, doi: 10.1109/TAP.2014.2330575.
[42] A. Madannejad, M. M. Gohari, U. Shah, and J. Oberhammer, "High-gain circularly polarized 500–750 GHz lens antenna enabled by silicon micromachining," *IEEE Trans. Antennas Propag.*, vol. 72, no. 5, pp. 4077–4085, May 2024, doi: 10.1109/TAP.2024.3383289.
[43] T. Deng, Y. Zhang, Z. Zheng, Q. Yan, and J. F. Mao, "High-gain and high-efficiency sub-terahertz antenna-on-chip with microbumps for highly-integrated systems," *IEEE Trans. Antennas Propag.*, vol. 72, no. 5, pp. 4107–4115, May 2024, doi: 10.1109/TAP.2024.3381444.
[44] H. Herdian, C. Wang, T. Inoue, A. Shirane, and K. Okada, "A proton irradiated CMOS on-chip Vivaldi antenna for 300 GHz band slat array implementation," *IEEE Open J. Antennas Propag.*, vol. 5, no. 5, pp. 1390–1402, Oct. 2024, doi: 10.1109/OJAP.2024.3422426.
[45] T. H. Lin et al., "Broadband and miniaturized antenna-in-package (AiP) design for 5G applications," *IEEE Antennas Wireless Propag. Lett.*, vol. 19, no. 11, pp. 1963–1967, Nov. 2020, doi: 10.1109/LAWP.2020.3018064.
[46] S. Erdogan, K. S. J. Moon, M. Kathaperumal, and M. Swaminathan, "D-band integrated and miniaturized Quasi-Yagi antenna array in glass interposer," *IEEE Trans. THz Sci. Technol.*, vol. 13, no. 3, pp. 270–279, May 2023, doi: 10.1109/TTHZ.2023.3242224.
[47] S. Erdogan, S. Ravichandran, X. Jia, and M. Swaminathan, "Characterization of chip-to-package interconnects for glass panel embedding (GPE) for sub-THz wireless communications," in *Proc. IEEE 71st Electron. Compon. Technol. Conf. (ECTC)*, 2021, pp. 2328–2333, doi: 10.1109/ECTC32696.2021.00364.
[48] X. Jia et al., "Antenna with embedded die in glass interposer for 6G wireless applications," *IEEE Trans. Compon. Packag. Manuf. Technol.*, vol. 13, no. 2, pp. 219–229, Feb. 2023, doi: 10.1109/TCPMT.2023.3251725.
[49] A. O. Watanabe et al., "Ultrathin antenna-integrated glass-based millimeter-wave package with through-glass vias," *IEEE Trans. Microw. Theory Techn.*, vol. 68, no. 12, pp. 5082–5092, Dec. 2020, doi: 10.1109/TMTT.2020.3022357.
[50] A. O. Watanabe, B. K. Tehrani, T. Ogawa, P. M. Raj, M. M. Tentzeris, and R. R. Tummala, "Ultralow-loss substrate-integrated waveguides in glass-based substrates for millimeter-wave applications," *IEEE Trans. Compon. Packag. Manuf. Technol.*, vol. 10, no. 3, pp. 531–533, Mar. 2020, doi: 10.1109/TCPMT.2020.2968305.
[51] M. Zhai, P. Bhaskar, H. Shi, M. Swaminathan, A. Locquet, and D. S. Citrin, "Terahertz characterization of glass-based materials and stackups for 6G microelectronics packaging," *J. Infrared, Millimeter, Terahertz Waves*, vol. 44, nos. 11–12, pp. 841–857, 2023, doi: 10.1007/s10762-023-00951-0.
[52] W. Hong, S. Lim, S. Ko, and Y. G. Kim, "Optically invisible antenna integrated within an OLED touch display panel for IoT applications," *IEEE Trans. Antennas Propag.*, vol. 65, no. 7, pp. 3750–3755, Jul. 2017, doi: 10.1109/TAP.2017.2705127.
[53] S. Y. Lee, D. Choi, Y. Youn, and W. Hong, "Electrical characterization of highly efficient, optically transparent nanometers-thick unit cells for antenna-on-display applications," in *Proc. IEEE/MTT-S Int. Microw. Symp. (IMS)*, Jun. 2018, pp. 1043–1045, doi: 10.1109/MWSYM.2018.8439303.
[54] J. Park et al., "Circuit-on-display: A flexible, invisible hybrid electromagnetic sensor concept," *IEEE J. Microw.*, vol. 1, no. 2, pp. 550–559, Apr. 2021, doi: 10.1109/JMW.2021.3063510.
[55] S. Beer, H. Gulan, C. Rusch, and T. Zwick, "Integrated 122-GHz antenna on a flexible polyimide substrate with flip chip interconnect," *IEEE Trans. Antennas Propag.*, vol. 61, no. 4, pp. 1564–1572, Apr. 2013, doi: 10.1109/TAP.2012.2232260.
[56] T. D. Nguyen, K. Kim, S. R. Yoon, and G. Byun, "Optically invisible artificial magnetic conductor subarrays for triband display-integrated antennas," *IEEE Trans. Microw. Theory Techn.*, vol. 70, no. 8, pp. 3975–3986, Aug. 2022, doi: 10.1109/TMTT.2022.3184688.
[57] D. Lee et al., "Dual-polarized dual-band antenna-on-display using via-less and single-layer topology for mmWave wireless scenarios," *IEEE Antennas Wireless Propag. Lett.*, vol. 22, no. 5, pp. 1000–1004, May 2023, doi: 10.1109/LAWP.2022.3230469.
[58] J. Park, I. Jang, B. Seong, and W. Hong, "Differentially fed, 1-D phased-array antenna-on-display featuring wideband and polarization agility for milli-

meter-wave wireless applications," *IEEE Trans. Antennas Propag.*, vol. 71, no. 9, pp. 7196–7205, Sep. 2023, doi: 10.1109/TAP.2023.3295448.
[59] D. Kim et al., "Characterization of nematic liquid crystal dielectric properties using complementary FSSs featuring electrically small cell gaps across a wide sub-THz range," *IEEE Trans. Antennas Propag.*, vol. 72, no. 2, pp. 2019–2024, Feb. 2024, doi: 10.1109/TAP.2023.3344274.
[60] Y. Youn et al., "Liquid-crystal-driven reconfigurable intelligent surface with cognitive sensors for self-sustainable operation," *IEEE Trans. Antennas Propag.*, vol. 71, no. 12, pp. 9415–9423, Dec. 2023, doi: 10.1109/TAP.2023.3312814.
[61] M. Sun, T. G. Lim, D. S. W. Ho, J. Wu, T. C. Chai, and Y. Ma, "77-GHz FOWLP MIMO AiP for compact high-resolution radar with horizontally and vertically long- and medium-range sensing," *IEEE Trans. Compon. Packag. Manuf. Technol.*, vol. 14, no. 4, pp. 537–546, Apr. 2024, doi: 10.1109/TCPMT.2024.3383463.
[62] T. Zhang et al., "A miniaturized vivaldi antenna in fan-out wafer-level package for 5G millimeter- wave applications," *IEEE Antennas Wireless Propag. Lett.*, vol. 23, no. 6, pp. 1914–1918, Jun. 2024, doi: 10.1109/LAWP.2024.3374365.
[63] X. Zhang, Q. Wang, C. Xia, C. Zhou, G. Wang, and J. Cai, "Fan-out antenna-in-package integration using heatsink antenna," *IEEE Trans. Compon. Packag. Manuf. Technol.*, vol. 12, no. 8, pp. 1262–1270, Aug. 2022, doi: 10.1109/TCPMT.2022.3195344.
[64] B. Yu et al., "A wideband mmWave antenna in fan-out wafer level packaging with tall vertical interconnects for 5G wireless communication," *IEEE Trans. Antennas Propag.*, vol. 69, no. 10, pp. 6906–6911, Oct. 2021, doi: 10.1109/TAP.2021.3087859.
[65] A. Fischer, Z. Tong, A. Hamidipour, L. Maurer, and A. Stelzer, "77-GHz multi-channel radar transceiver with antenna in package," *IEEE Trans. Antennas Propag.*, vol. 62, no. 3, pp. 1386–1394, Mar. 2014, doi: 10.1109/TAP.2013.2294206.
[66] D. Lee et al., "Planar asymmetric fed interdigital coupling antenna-in-package using FOWLP process operating at 60–90 GHz in endfire mode," *IEEE Trans. Microw. Theory Techn.*, vol. 72, no. 4, pp. 2378–2390, Apr. 2024, doi: 10.1109/TMTT.2023.3347740.
[67] Z. Yang, C. Y. Ko, and S. Ramanathan, "Oxide electronics utilizing ultrafast metal-insulator transitions," *Annu. Rev. Mater. Res.*, vol. 41, no. 1, pp. 337–367, 2011, doi: 10.1146/annurev-matsci-062910-100347.
[68] M. Lust, S. Chen, C. E. Wilson, J. Argo, V. Doan-Nguyen, and N. Ghalichechian, "High-contrast, highly textured VO_2 thin films integrated on silicon substrates using annealed Al_2O_3 buffer layers," *J. Appl. Phys.*, vol. 127, no. 20, 2020, Art. no. 205303, doi: 10.1063/1.5144816.
[69] J. Leroy, A. Crunteanu, A. Bessaudou, F. Cosset, C. Champeaux, and J. C. Orlianges, "High-speed metal-insulator transition in vanadium dioxide films induced by an electrical pulsed voltage over nano-gap electrodes," *Appl. Phys. Lett.*, vol. 100, no. 21, 2012, Art. no. 213507, doi: 10.1063/1.4721520.
[70] S. Yang, W. Li, M. Vaseem, and A. Shamim, "Fully printed VO_2 switch based flexible and reconfigurable filter," in *Proc. IEEE/MTT-S Int. Microw. Symp. (IMS)*, 2020, pp. 49–52, doi: 10.1109/IMS30576.2020.9224095.
[71] N. El-Hinnawy, G. Slovin, J. Rose, and D. Howard, "A 25 THz F_{CO} (6.3 fs $R_{ON} * C_{OFF}$) phase-change material RF switch fabricated in a high volume manufacturing environment with demonstrated cycling > 1 billion times," in *Proc. IEEE/MTT-S Int. Microw. Symp. (IMS)*, 2020, pp. 45–48, doi: 10.1109/IMS30576.2020.9223973.
[72] E. Carrasco and J. Perruisseau-Carrier, "Reflectarray antenna at terahertz using graphene," *IEEE Antennas Wireless Propag. Lett.*, vol. 12, pp. 253–256, 2013, doi: 10.1109/LAWP.2013.2247557.
[73] C. Jin, V. N. Sekhar, X. Bao, B. Chen, B. Zheng, and R. Li, "Antenna-in-package design based on wafer-level packaging with through silicon via technology," *IEEE Trans. Compon. Packag. Manuf. Technol.*, vol. 3, no. 9, pp. 1498–1505, Sep. 2013, doi: 10.1109/TCPMT.2013.2261855.
[74] D. Malta et al., "TSV-last, heterogeneous 3D integration of a SiGe BiCMOS beamformer and patch antenna for a W-band phased array radar," in *Proc. IEEE 66th Electron. Comp. Tech. Conf. (ECTC)*, 2016, pp. 1457–1464, doi: 10.1109/ECTC.2016.103.
[75] S. R. Govindarajulu, R. Hokayem, and E, and A. Alwan, "A 60 GHz millimeter-wave antenna array for 3D antenna-in-package applications," *IEEE Access*, vol. 9, pp. 143,307–143,314, 2021, doi: 10.1109/ACCESS.2021.3121320.
[76] S. D. Lee et al., "Wideband, high efficiency on-chip monolithic integrated antenna at W-band using miniaturized cavity and through silicon via," *IEEE Trans. Compon. Packag. Manuf. Technol.*, vol. 14, no. 12, pp. 2355–2363, Dec. 2024, doi: 10.1109/TCPMT.2024.3495520.
[77] C. Okoro, J. W. Lau, F. Golshany, K. Hummler, and Y. S. Obeng, "A detailed failure analysis examination of the effect of thermal cycling on Cu TSV reliability," *IEEE Trans. Electron Devices*, vol. 61, no. 1, pp. 15–22, Jan. 2014, doi: 10.1109/TED.2013.2291297.
[78] X. Liu et al., "Thermo-mechanical behavior of through silicon vias in a 3D integrated package with inter-chip microbumps," in *Proc. IEEE 61st Electron. Compon. Technol. Conf. (ECTC)*, 2011, pp. 1190–1195, doi: 10.1109/ECTC.2011.5898661.
[79] V. Pano, I. Tekin, I. Yilmaz, Y. Liu, K. R. Dandekar, and B. Taskin, "TSV antennas for multi-band wireless communication," *IEEE J. Emerg. Sel. Top. Circuits Syst.*, vol. 10, no. 1, pp. 100–113, Mar. 2020, doi: 10.1109/JETCAS.2020.2974236.
[80] S. Oh, T. Zheng, and M. S. Bakir, "Electrical characterization of shielded TSVs with airgap isolation for RF/mmWave applications," *IEEE Trans. Compon. Packag. Manuf. Technol.*, vol. 14, no. 2, pp. 202–210, Feb. 2024, doi: 10.1109/TCPMT.2024.3358102.
[81] S. Hu, Y. Z. Xiong, L. Wang, R. Li, J. Shi, and T. G. Lim, "Compact high-gain mmWave antenna for TSV-based system-in-package application," *IEEE Trans. Compon. Packag. Manuf. Technol.*, vol. 2, no. 5, pp. 841–846, May 2012, doi: 10.1109/TCPMT.2012.2188293.
[82] B. Sadhu et al., "A 24–30-GHz 256-element dual-polarized 5G phased array using fast on-chip beam calculators and magnetoelectric dipole antennas," *IEEE J. Solid-State Circuits*, vol. 57, no. 12, pp. 3599–3616, Dec. 2022, doi: 10.1109/JSSC.2022.3204807.
[83] X. Gu et al., "Development, implementation, and characterization of a 64-element dual-polarized phased-array antenna module for 28-GHz high-speed data communications," *IEEE Trans. Microw. Theory Techn.*, vol. 67, no. 7, pp. 2975–2984, Jul. 2019, doi: 10.1109/TMTT.2019.2912819.
[84] W. Hong et al., "Multibeam antenna technologies for 5G wireless communications," *IEEE Trans. Antennas Propag.*, vol. 65, no. 12, pp. 6231–6249, Dec. 2017, doi: 10.1109/TAP.2017.2712819.